Urol Res (1984) 12:17–22

Urological Research

Electron Microscopy of Urinary Calculi – Some Facts and Artefacts

D. Crawford

Electron Microscope Unit, R. W. James Building, University of Cape Town, Rondebosch, South Africa

Accepted: October 24, 1983

Summary. Material in urinary calculi is prone to irradiation damage during electron microscopy and this suggests the need for care in the interpretation of data. It is shown, however, that minimum-dose transmission microscopy is feasible for single-crystal electron diffraction work, and that although internal damage in severe, morphological artefacts are unlikely in the SEM unless the incident electron flux is greater than 10^{-13} A nm^{-2}. During EDX microanalysis, the detection of light elements is impaired by irradiation effects unless a minimum-dose procedure is used. For the preparation of SEM samples, artefacts can be created by cleaving air-dried material – and it is therefore important to consider more lengthy preparation methods such as cryogenics.

Key words: Urinary calculi, Electron microscopy, X-ray microanalysis, Artefacts.

Introduction

Following work by Spector [8], the scanning electron microscope (SEM) operating in the secondary electron or X-ray microanalytical mode, is now established as a viable method for the investigation of structure in urinary calculi. Rodgers [7] for example, notes the value of easily-obtainable morphological observations for the determination of growth mechanisms in calculi. However, whereas it is generally accepted that large-scale morphology is well-represented in secondary-electron images, there are doubts concerning the interpretation of fine detail [9]. Such doubts arise because it is well-known that structural transformations occur in weakly-bonded materials as a result of electron-irradiation damage: in turn, the induced structural changes may lead to unpredictable alterations of the fine morphology. When such events occur, the results can be dramatic; for example, during a mineralogical SEM investigation of goethite (∝FeO.OH) a bulky isometric precursor can be transformed, upon electron impact, to needle crystals [3].

The appearance of a morphological change during microscopy is therefore a symptom of structural re-arrangement, but it is unsafe to assume that in the absence of an observed change in morphology there is no irradiation damage. Structural changes without morphological changes occur typically during the degradation of crystals into amorphous material, and have been observed for example during microscopy of hydrated zeolites [2]. In this case, the postulated loss of free hydrogen [4] would not have affected a simultaneous qualitative X-ray microanalysis (had it been performed), but it is likely that other damage-prone materials could exhibit a mass loss or diffusion of important and detectable ions. The difficulties associated with probe damage of mineralogical sulphides, for example, are well known to geologists.

It is therefore incorrect to assume that easily-interpretable data can be obtained from X-ray energy dispersive microanalysis (EDX) and secondary electron imaging at higher resolution. As others have suggested [4, 10] there are certain aspects of SEM urological research that cannot be attempted with any reasonable degree of confidence without prior knowledge of induced artefacts. In this paper we show that a knowledge of induced effects can lead to alternative and better methods for investigating calculi.

Materials and Methods

The observations were made during an investigation of constituents and morphology in a collection of nine small spontaneously-passed calcium kidney stones which were air dried after collection. In an attempt to investigate and explain some puzzling observations made during routine scanning electron microscopy, baseline experiments were conducted using the transmission electron microscope (TEM) and the results were extrapolated to the scanning electron microscope (SEM). Thus, the TEM was used initially to acquire data on irradiation damage. As a consequence of that investigation it was shown that by using characterized minimal irradiation doses, the

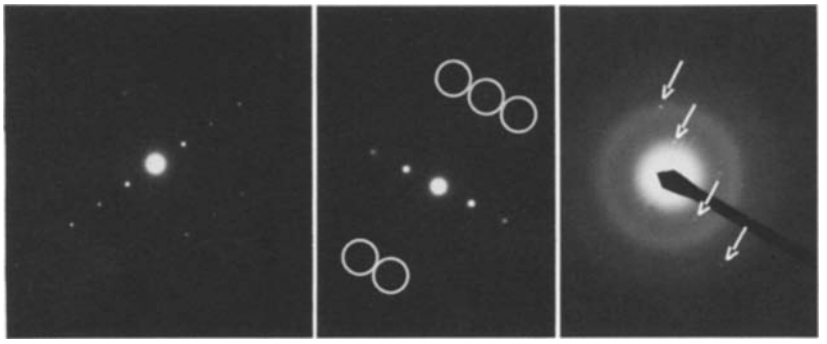

Fig. 1 (Left). An electron diffraction pattern recorded from a thin fragment of $CaC_2O_4 \cdot H_2O$ using 200 keV electrons and a dose of about 300 $e^{-}nm^{-2}$

Fig. 2 (Centre). An electron diffraction pattern recorded from a thin crystal of either $CaC_2O_4 \cdot H_2O$, $MgHPO_4 \cdot 3H_2O$, or $Ca_4H(PO_4)_3 \cdot 2.5H_2O$. Weak reflections are circled

Fig. 3 (Right). An electron diffraction pattern recorded using a minimum electron dose for $CaHPO_4 \cdot 2H_2O$. The diffuse rings indicating a low degree of crystalline order are punctuated by sharp spots (*arrowed*) which suggest the presence of a small number of extensive crystals in the poorly-ordered matrix

TEM itself could be used to investigate the feasibility of identifying single-crystal components (by electron diffraction), and the SEM could be used to investigate the effects of probe damage during routine X-ray microanalysis.

Transmission Electron Microscopy

Samples were ground for 5 min in a dry agate mortar and pestle before being dusted on to a 200-mesh copper grid containing a holey supporting film made of Au/Pd-coated formvar. Using the double-tilt goniometer on a JEOL 200CX TEM, samples were evacuated in the pumped chamber overnight and subsequently they were surveyed at sub-minimal exposure levels [6] using an undersaturated filament to reduce the electron flux, and a grossly underfocused image to create contrast. Electron diffraction patterns (EDP) or images were recorded on Kodak 4489 emulsion using electron-dose levels calibrated to ± 10% using the known response of dry photographic emulsion under standard developing conditions.

Initially, crystals were identified by sight and those fragments bridging holes in the formvar film were chosen for recording an electron diffraction pattern at a low-dose level. Subsequently, the image was recorded in the same low-dose condition and this was followed by repeated EDP and image recording which gave a series characterising structural changes at defined electron doses. This sequence was repeated at different accelerating potentials until a set of results was obtained for calcium oxalate monohydrate (COM) and for calcium oxalate dihydrate (COD).

The single-crystal EDPs were indexed automatically using a computer programme (Crystal4) implemented on a Univac 1100 mainframe computer. The programme takes the coordinates of 3 reflections in a zone-axis diffraction pattern and matches them to predicted reflections from known suspect materials in all the possible zone-axis orientations. The match is performed on the basis of experimental errors, and the ensuing results, showing a full indexing system and the viewed zone-axis, contain deviation parameters (suspect/unknown) so that the most probable fit can be determined if necessary.

Scanning Electron Microscopy

One half of each fractured stone was mounted, with the freshly-cleaved surface facing upwards, on a graphite disc. The disc was then attached to an aluminium series-100 stub for Cambridge scanning electron microscopes.

Non-volatile glue was used as a mounting medium throughout the experiment, and the conduction path between graphite and the aluminium stub, being interrupted by the glue, was reformed with a dab of Silverdag colloidal silver. In one case of microanalysis, a stone was removed from the stub after conventional SEM work and mounted in Epon resin before curing at 333K to produce a block for polishing using 7, 2 and 0.1-micrometer silica paste on Selvyt cloth.

Cleaned and mounted samples were coated with about 80 nm of carbon evaporated at a vacuum pressure of 3 mPa in a Balzer's vacuum coater equipped with a planetary rotating specimen holder.

Some samples were examined using a Cambridge S180 SEM operating in secondary-electron imaging conditions at a probe current of 6×10^{-11} Amps. Concomitant X-ray analysis was performed using either a Kevex or an Edax horizontal detector. Of particular note, the S180 was equipped with a tantalum final aperture and carbon-coated chamber components; this eliminated spurious X-ray collection but spectra were still subjects to systematic faults (e.g. the Si internal fluorescence peak), so the equipment was carefully characterised prior to the acquisition of data.

Other samples, depending on their nature and the behaviour of control material, were imaged under heavy or light probe currents in the SEM. For the polished sample, a special low-dose method was used to acquire an X-ray spectrum. Details of that method are given in a later section of this paper.

Results

1. Electron Diffraction

(i) Identification of Crystals. Using 200 KeV electrons and a dose of $<200e^{-}$ nm^{-2}, electron diffraction patterns were recorded for single-crystal oxalates and polycrystals of phosphates in the powdered samples. Automatic indexing in a match routine contained in the crystal4 programme, works strictly on the basis of estimated experimental errors and it attempts to identify common suspect materials. Using one electron diffraction pattern from a single crystal may give a fortuitously unambiguous identification such as the calcium oxalate monohydrate crystal (COM) in Fig. 1 and Table 1. However, with certain suspect components the unit cell projections can be very similar and therefore within experimental errors, ambiguities can arise. For example, for the electron diffraction pattern shown in Fig. 2, there are 8 indexing possibilities for calcium oxalate monohydrate (COM), 7 for octacalcium phosphate and 8 for magnesium hydrogen phosphate trihydrate. Although the single-crystal nature of the specimen, and smaller EDP errors, indicate that Newberyite is most probable (Table 2), it is clear that 2 or 3 zone axes should be indexed for each crystal when

Table 1. The results of an auto-indexing programme applied to three reflections in the e.d.p. of Fig. 1. The programme matched calcium oxalate monohydrate in a [−1, 0, 0] zone axis orientation after consideration of 10 suspect crystals – $CaC_2O_4 \cdot H_2O$, $CaC_2O_4 \cdot 2H_2O$, $Ca_{10}(PO_4)_6(OH)_2$, $MgNH_4PO_4 \cdot 3H_2O$, $CaHPO_4 \cdot 2H_2O$, $Ca_4H(PO_4)_3 \cdot 2.5H_2O$, $MgHPO_4 \cdot 3H_2O$, $C_5H_4N_4O_3$, $C_5H_4N_4O_3 \cdot 2H_2O$, cystine $(-SCH_2CHNH_2COOH)_2$

Analysis using COM Suspect

given Lambda * L = 16.1 + or − 1.5%

R (mm)	Angles	Indices	R deviation
4.43	37.50	040	0.001
2.78	90.00	021	0.000
3.38	52.50	002	0.000
Beam axis is		−1,0,0	

R = distance on plate (000) – to – (reflection)
Angles = measured angles between reflections
Indices = best-fit Miller indices for reflections
R deviation = deviation of the reciprocal lattice vector calculated on the basis of the best-fit Miller Indices, from that measured (by R)
Beam axis = the zone axis indices for the best-fit Miller indices

rigorous identifications are necessary – indeed, this is normal practice for beam-stable materials.

For the case of polycrystals, identification is performed by necessity, on the basis of powder diffraction patterns only. Fig. 3 is a typical EDP obtained from a sample of hydroxyapatite.

It should be noted that during this investigation, several single crystals could not be indexed using the unit-cell dimensions for the pure stone-forming compounds. This suggests that the unit cell of certain compounds were significantly distorted by impurities; alternatively, there could be unusual crystals in some of the nine samples chosen for investigation.

(ii) Damage Induced by the Electron Probe. The structural damage induced by the electron probe is illustrated in EDPs shown in Fig. 4 for the case of 200 keV electrons incident on a thin single crystal. The rate of loss of structural order depends upon the orientation of the crystal to the electron probe. However, for COM and COD, all the crystalline reflections are lost after a dose between 400 and 550 $e^- nm^{-2}$ at 200 keV. Data for other probe energies is given in Fig. 5.

Table 2. The indexing possibilities for the e.d.p. of Fig. 2. The programme attempted matching to the 10 crystals mentioned in the legend to Table 1, and found that within experimental errors COM, OCTACALC and NEWBER were possible. The smaller mean R-deviations for NEWBER indicate that Newberyite is the most probable suspect

Analysis pattern No. 3 (i.e. that in Fig. 2)

given Lambda * L = 16.1 + or − 1.5%

Analysis using COM suspect

Beam axis possibilities & mean R-deviation per axis

(−5 −5 −1) ... 0.004	(5 −5 1) ... 0.004	(−2 −1 −1) ... 0.004
(−2 1 −1) ... 0.003	(−1 −1 0) ... 0.004	(1 −1 0) ... 0.004
(4 5 −1) ... 0.004	(−4 5 1) ... 0.004	

Analysis using OCTACALC suspect

Beam axis possibilities & mean R-deviation per axis

(5 −3 3) ... 0.003	(2 1 1) ... 0.004	(3 2 2) ... 0.007
(−6 −5 1) ... 0.005	(3 1 1) ... 0.004	(−5 3 3) ... 0.005
(−3 −2 1) ... 0.006		

Analysis using NEWBER suspect

Beam axis possibilities & mean R-deviation per axis

(4 0 3) ... 0.002	(−1 0 0) ... 0.002	(1 0 5) ... 0.002
(−3 0 4) ... 0.004	(−4 0 3) ... 0.002	(−1 0 5) ... 0.002
(3 0 4) ... 0.004	(0 0 1) ... 0.006	

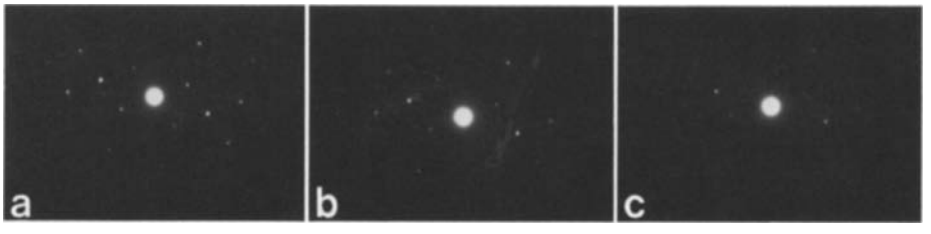

Fig. 4. Electron diffraction patterns recorded from a single crystal after a) 150 $e^- nm^{-2}$, b) 300 $e^- nm^{-2}$, c) 450 $e^- nm^{-2}$ at 200 kV. Measurements of electron doses are subject to ± 10% error. This series of images is a phenomenological demonstration of the loss of crystallinity with increasing electron dose

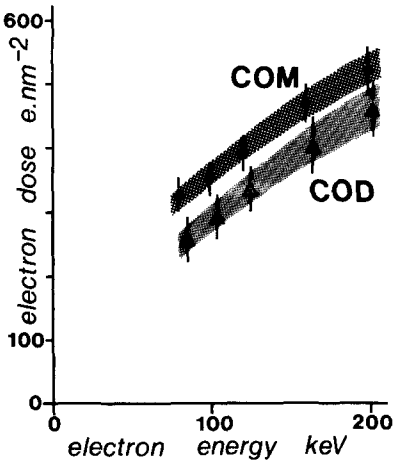

Fig. 5. A graph showing the electron dose required to destroy crystallinity in $CaC_2O_4 \cdot H_2O$ (COM) and $CaC_2O_4 \cdot 2H_2O$ (COD) for electron probes in the energy range 80–200 keV

2. Transmission-Electron Images

Undamaged crystals of COM and hydroxyapatite are shown in Fig. 6. Calcium oxalates exhibit mass loss during electron irradiation and damage is characterised by the appearance of voids (Fig. 7) which follows the degradation of crystallinity. Polycrystalline hydroxyapatite is recrystallised by electron irradiation at 40,000 $e^- nm^{-2}$; and from a poorly-crystallised precursor, a sharply-crystalline product emerges. The ensuing crystals, being quite stable to the electron probe, can be imaged quite successfully at high resolution (Fig. 8). During recrystallisation, fine morphology is eliminated since several polycrystals dissolve together and there may be some shrinkage. However, the effective change in morphology is apparent only at levels of resolution better than the natural aggregate size of hydroxyapatite.

3. Scanning Electron Microscopy

(i) Artefacts Created by Specimen Preparation. Probe-induced morphological changes were not observed on any of the nine stones examined at 15 KeV using probe currents set at 6×10^{-11} Amps and SEM resolution of about 28 nm. However, some very unusual beamstable morphologies were observed and are thought to arise during specimen preparation.

One stone showing a COM bulk morphology but for which single-crystal electron diffraction patterns were difficult to index, revealed fibrous crystal growths (Fig. 9) apparantly extending radially from deposits containing calcium and phosphorous (ie) probably a calcium phosphate. Another stone exhibited many phosphorus-rich protrusions from COM-like substrates (Fig. 10). The latter detail was not observed during preliminary SEM work done immediately after preparation and carbon coating, but was noted on subsequent examination 6 days later.

(ii) Artefacts Created by Heavy Electron Doses. Using an unecessarily high probe current for imaging, but usual levels (1×10^{-10} A) for X-ray microanalysis of stable material, surface bubbles were created on crystals having the external appearance of COD. COM however, and phosphate deposits were morphologically stable at the operating resolution.

4. X-ray Microanalysis

Bearing in mind the structural changes and the mass loss to be expected with COM, COD and hydroxyapatite, a careful low-dose SEM microanalysis was undertaken on the polished surface of a stone. Monte-Carlo simulations show that the interaction volume for a 10 keV electron probe incident

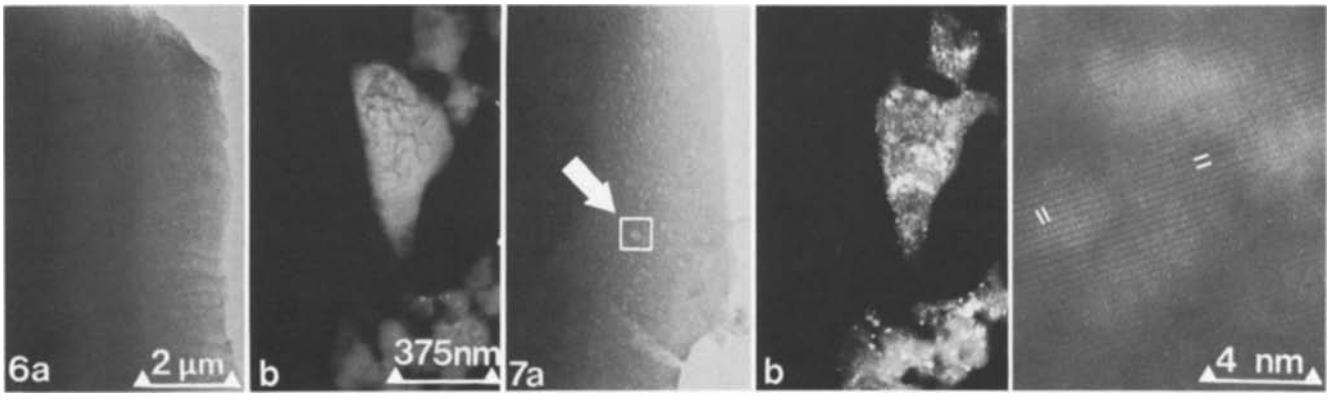

Fig. 6a, b. Undamaged COM and hydroxyapatite recorded using minimum electron doses. **a** bright-ground image of COM; **b** dark-ground image of hydroxyapatite (the lack of sharp white dots indicates low crystallinity c.f. Fig. 7b)

Fig. 7a, b. Damaged crystals of COM and hydroxyapatite. **a** bright-ground image of COM showing large voids (*arrowed*); **b** dark-ground image of hydroxyapatite (the proliferation of white dots is indicative of crystallinity c.f. Fig 6b). Scales are the same as Fig 6

Fig. 8. A high-resolution TEM image showing lines which represent the atomic planes in an extensive crystal produced by recrystallisation of a hydroxyapatite deposit

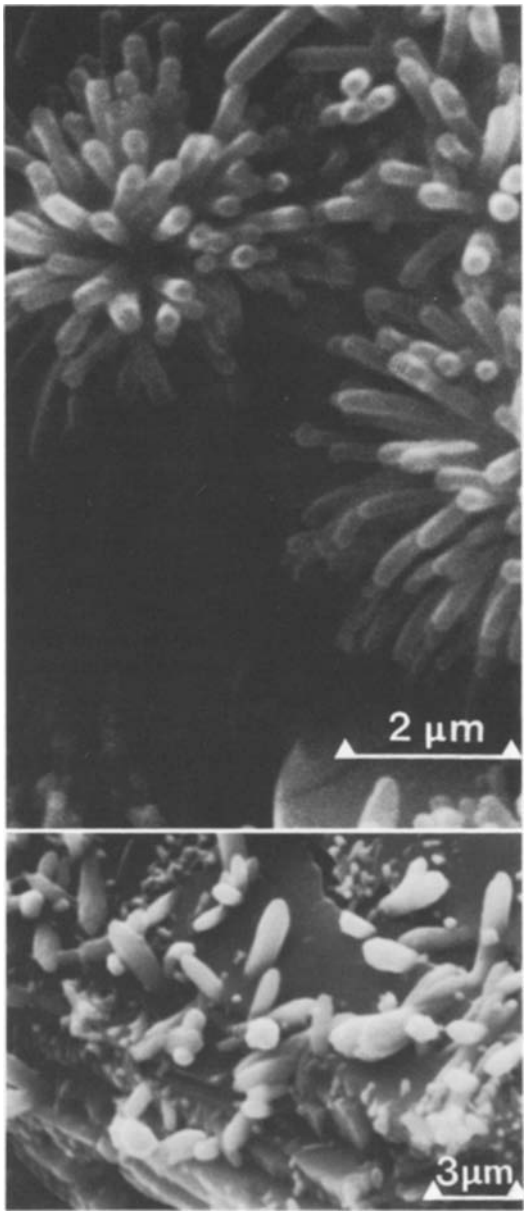

Fig. 9. SEM micrograph illustrating radial growths from a P-rich substrate. The fibrous material is thought to be an artefact resulting from a bad preparation strategy

Fig. 10. SEM micrograph illustrating P-rich protrusions from a COM substrate. These protrusions were not observed during microscopy immediately after preparation, but were observed and recorded in a microscopy session 6 days later

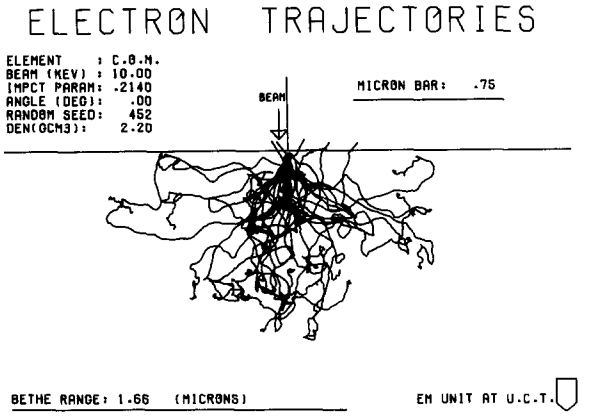

Fig. 11. A simple Monte-Carlo plot of electron trajectories in COM. The 10 keV electron probe spreads by about 1.5 µm in the sample

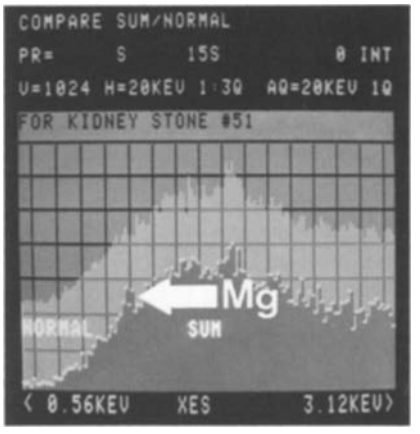

Fig. 12. A comparison of a normal EDX spectrum acquired using a stationary spot mode of analysis for 150 s and a special EDX spectrum which is the sum of 10 separate 15 s acquisitions – each on fresh material. A Mg Kα peak (present at the 65% confidence level) is arrowed in the summed spectrum but cannot be seen in the normal spectrum

on COM is about 1.5 micrometers wide (Fig. 11) for a sample density of 2.2 gms cm^{-3}. Accordingly, on a blind area previously unirradiated, several 15 second X-ray acquisitions were made using spot analyses separated by at least 2 micrometers. A probe current of 1×10^{-10} Amps allowed sufficient X-ray collection in the S180 SEM with a horizontal 30 mm^2 detector and an inclined sample. The summation spectrum of all these acquisitions was compared with the spectrum of an adjacent area acquired for the same total time. It is seen from Fig. 12 that the summed spectrum contains an Mg peak (identified at a 65% confidence level) whereas the normal spectrum does not. Bremsstrahlung count rates at a 0.9–1.0 keV window were monitored during subsequent normal acquisitions in spot mode using different probe currents. Fig. 13 illustrates that 6×10^{-11} Amps gives a stable count rate on COM whereas 1×10^{-10} Amps gives a reduction of count rate in the first 20 seconds of the acquisition; this suggests a serious mass loss at the higher probe current.

Discussion

Considering COM and COD components in kidney stones, the TEM experiments show that there is severe structural damage at low levels of incident radiation in the microscope. Extrapolating the data given in Fig. 5 to the range of electron energies used in tlhe SEM (5–35 keV), it is apparent that the upper limit for damage is in the range 200–300 $e^- nm^{-2}$. In a SEM operating with a probe area of 600 nm^{-2} and a current of 6×10^{-11} Amps, this condition means that

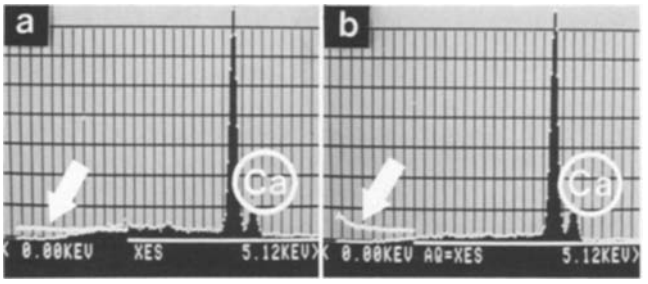

Fig. 13a, b. These spectra for COM were acquired in a normal conditions of 6×10^{-11} amps probe current, and b heavy dose conditions of 1×10^{-10} amps probe current. The *arrowed* white plot is a graph of X-ray counts (*ordinate*) versus time (*abscissa*) in a low energy window. For the heavy dose, X-ray counts are lost, indicating a mass loss of material

severe damage on an atomic scale will occur after a dwell period shorter than 1 μs. With 1,000 lines/frame, microstructure therefore will be disrupted after one scan frame of duration 1 s! In the normal situation of pre-viewing, focusing and recording in the SEM, the electron dose exceeds this damage condition by factors of 100 or more. So, it is certain that atomic order in COM and COD is destroyed during normal scanning electron microscopy: further, using information from Fig. 7 it can be expected that voids are gradually developed with increasing dose until a noticeable state of reduced density is developed at about 1,000 e nm^{-2} in the SEM (1 frame of 8 s duration). The bubble effects observed in the SEM used at high probe currents are probably the result of massive and sudden volatilisation – this opinion is evidence by the drop in the monitored X-ray count rate at 1×10^{-10} Amps (Fig. 13).

Despite the extra resistance of hydroxyapatite (present as very poorly crystalline aggregate material), a similar assessment shows that for the same SEM scenario, the recrystallisation depicted in Fig. 7b will occur after 100 scan frames of duration 1 s (i.e. 100 s fullframe exposure). Therefore it is equally clear that hydroxyapatites change their form under the SEM probe.

As far as the identification of kidney stone components is concerned, it seems that the damage effects are unlikely to cause a radical error in observations of SEM images. However, this is not the case for X-ray microanalysis because this experiment shows that the detection of minor quantities of Mg can be impaired by using a single-spot technique and continuous acquisition. It is far better, where possible, to attempt to avoid the possibilities of high rates of volatilization and ionic migration by using methods which rely on the summation of several data acquisitions from volumes previously unirradiated in the same sample. This is amply demonstrated by the results shown in Fig. 12. In this case, since several very noisy spectra are to be summed, it is very important to check the Poisson counting statistics of the multi-channel analyser incorporated into the X-ray equipment. Where it is not possible to perform such analysis, the acquired X-ray data may not reveal the true chemical nature of minor constituents in the sample.

EDP is a rigorous method of identifying microconstituents and with careful minimum-dose TEM methods at 200 keV, two zone-axes can be recorded ($\sim$200 $e^- nm^{-2}$ per axis) for single crystals before the crystalline order is lost ($\sim$500 $e^- nm^{-2}$). However, EDP does not allow a visualisation of the inter-relationship of components, hence both TEM and SEM should be used as complementary tools.

Turning now to the most serious source of artefacts revealed in the present work (Figs. 9 and 10), it is apparent that consideration must be given to methods of preparation. The mechanism which produces the artefacts is unknown – however, hydration of glass is known to cause surface growths [1] which show an apparent Arrhenius behaviour. A similar effect is likely on rehydration of the inner surfaces of kidney stones originally having gel constituents such as the poorly-ordered hydroxyapatites – and thus, low temperatures should retard the growth of artefacts. Hence the best strategy for SEM preparation should not only involve freeze – or critical point drying, but also cryo-fracturing. It is recommended that samples should be examined without delay after the preparation since it appears that the growth of artefacts may in some stones occur in a few days.

Acknowledgements. I want to record that my work in electron microscopy of kidney stones began in association with the late Dr. M. Modlin. Many thanks to Dane Gerneke for technical support beyond the requirements of his job.

References

1. Bates JK, Jardine LJ, Steindler MJ (1982) Hydration aging of nuclear waste glass. Science 218:51–54
2. Bursill LA, Thomas JM, Rao KJ (1981) Stability of zeolites under electron irradiation and imaging of heavy cations in silicates. Nature 289:157–158
3. Calvo FA, Guilemany JM, Gomez De Salazar JM (1980) The contribution of SEM – EDAX and EPMA to the study of the structure and genesis of Spanish mercury ores. Proc Electron Microscopy 1980, The Hague, pp 456–457
4. Hirsch EH (1981) Matters – arising from stability of zeolites under electron irradiation. Nature 293:759
5. Meyer AS, Finlayson B, DuBois L (1971) Direct observation of urinary stone ultrastructure. Br J Urol 43:154–163
6. Misell DL (1978) Image analysis, enhancement and interpretation. North-Holland, Amsterdam New York Oxford, pp 11–14
7. Rodgers AL, Nassimbeni LR, Mulder KJ (1982) A multiple technique approach to the analysis of urinary calculi. Urol Res 10:177–184
8. Spector M, Jameson LH (1976) Scanning electron microscopy of urinary calculi. Proc SEM 1976 IIT Research Institute Chicago, pp 307–314
9. Spector M, Garden N, Rous S (1978) Ultrastructure and pathogenesis of human urinary calculi. Br J Urol 50:12–15
10. Spector M, Lilga JC (to be published) High voltage electron microscopy of urinary calculi.

Dr. D. Crawford
Electron Microscope Unit
R. W. James Building
University of Cape Town
Rondebosch
South Africa